Nanomed J. 12(1): 18-32, Winter 2025

RESEARCH PAPER

Fabrication of a fast response non-enzymatic glucose sensor based on in-situ synthesized Cu-metal organic frameworks integrated with electrochemically reduced graphene quantum dots

Samaneh Makani [1], Biuck Habibi [1]*, Rahim Mohammad-Rezaei [1]

[1]Electrochemistry Research Laboratory, Faculty of Basic Sciences, Azarbaijan Shahid Madani University, Tabriz, Iran

ABSTRACT

Objective(s): During this study, a novel and fast response platform based on in-situ synthesis of Cu-metal organic frameworks (Cu-MOFs) integrated with electrochemically reduced graphene quantum dots (ErGQDs) was developed through an electrochemical deposition method and a conversation process for non-enzymatic glucose determination.

Materials and Methods: In the first step, metallic copper and ErGQDs were simultaneous electrochemically deposited on the surface of carbon ceramic electrode (CCE). Then, metallic copper was converted to copper oxide by cyclic voltammetry technique. Finally, by adding the benzene-1, 3, 5-tricarboxylic acid (BTC), copper-based MOFs was formed on the surface of constructed electrode by an in-situ conversation process and the fabricated electrode (Cu-MOFs/ErGQDs/CCE) was used for the non-enzymatic electrochemical detection of glucose. The physicochemical characterization and electrocatalytic behavior of fabricated electrode toward glucose oxidation were studied through the suitable techniques.

Results: The electrochemical results demonstrated that the Cu-MOFs/ErGQDs/CCE is a suitable sensor for glucose determination which exhibits wide linear ranges (2.0-500.0 μM), low detection limit [0.59 μM (S/N=3)], high sensitivity (5069 μA mM-1cm-2), stability (RSD%=3.02), reproducibility (RSD%= 2.09) and good selectivity.

Conclusion: Overall, this study highlights the development of Cu-MOFs/ErGQDs/CCE as a sensor with promising characteristics for non-enzymatic determination of glucose. So that, the present sensor was used for detection of glucose in human blood serum and saliva samples.

Keywords: *Copper-metal organic frameworks, Carbon ceramic electrode, Electrochemical detection, Glucose, Reduced graphene quantum dots*

How to cite this article

Makani S, Habibi B, Mohammad-Rezaei R. Fabrication of a fast response non-enzymatic glucose sensor based on in-situ synthesized Cu-metal organic frameworks integrated with electrochemically reduced graphene quantum dots. Nanomed J. 2025; 12: 18-32. DOI: 10.22038/nmj.2024.75527.1833

INTRODUCTION

Metal-organic frameworks (MOFs) are a unique category of tunable porous materials composed of metal ions coordinated to organic ligands that have been well-tried to be used in countless fields such as sensing device, electrocatalysis, chemical separation, gas adsorption, supercapacitors, drug delivery and etc due to their adjustable and unique properties like high available surface area and ordered crystalline structure [1-3]. Various methods such as microwave-induced [4], solvothermal [5], seeded growth [6], layer by layer deposition [7], electrochemical deposition [8, 9] and in situ growth methods [10, 11] have been reported for deposition of MOFs on the surface of electrodes and electrical devices. Compared to other synthetic procedures used for the formation of MOFs on the surface of electrodes, in-situ synthesis method seems to be a remarkably easier and acceptable method due to the facile synthesis by conversion, without any need for much time and special condition [10-12]. Therefore, it seems

* *Corresponding author: Email: B.Habibi@azaruniv.ac.ir*

Note. This manuscript was submitted on October 11, 2023; approved on March 11, 2024

that the MOFs can be effectively used to modify solid surfaces such as carbon ceramic electrode (CCE), which is widely used in electrochemistry owing to their high mechanical and chemical stability, renewable surface, and wide potential window [13, 14]. However, the constitutional imperfection and low electrical conductivity of the pure MOFs led to their lack of acceptable behavior in electrochemical applications [3, 15]. To resolve these problem and growth the steadiness and usefulness of MOFs, they are integrated with various functional materials to improve their electrochemical performances and stability compared to pure MOFs [16-18]. In recent studies, combinations of MOFs with graphene quantum dots (GQDs) was used and their multiple interactions elevated [19]. GQDs are small (less than 100 nm) two-dimensional graphene flakes with ideal properties such as higher surface-to-volume ratio, strong chemical effect, and excellent optical stability also; they are high biocompatibility and non-toxic [20]. Due to the presence of various functional groups on the surface of GQDs such as carbonyl groups, hydroxyl groups and amino acids, has good solubility in aqueous media, and is a good electron transporter and acceptor too [21]. Thanks to strong π-π interactions, they can interact with other substances, inorganic and biological nanostructures and their unique properties are merged due to the hydrogen bonding, π-π stacking and metal-O coordination between MOFs and GQDs [22]. This is an effective strategy to improve the essential properties of MOFs and increase their signal as a modifier in electrochemical sensors. Recently, some papers have reported on the reduction of graphene quantum dots (GQDs) to reduced graphene quantum dots (rGQDs) through the use of reducing agents [23, 24]. The reduction process involves the elimination of excessive functional groups, which in turn reduces the energy band gap and enhances the electron transfer properties. Due to the more negative conduction band of GQDs in comparison to the linkers present in MOFs, a donor-acceptor charge transfer can be observed from the electron-donating GQDs to the electron-retreating linkers [25]. Consequently, the hybrid materials containing rGQDs and MOFs exhibit superior electrochemical sensing activity when compared to both pristine GQDs and MOFs [12, 15, 22]. Additionally, the inherent ultrahigh surface areas and porosities of MOFs confer advantages that facilitate mass transfer and accumulation of target analytes, thereby leading to a rapid response during the sensing process. On the other hand, considering the extensive benefits and additionally complementary and synergetic results among MOFs and rGQDs, the combination of MOFs and rGQDs can be used to improve the performance of the designed sensors [12, 22].

On the other hand, as known diseases such as diabetes has become a global epidemic today, due to the complications and consequences of this issue, it typically causes people to die. Therefore, it is better to diagnose the disease in the early stages [26]. The World Health Organization (WHO) also estimates significant deaths toll from diabetes annually. Scientific and research studies in this field are expected to expand. The glucose level of human blood could be a crucial signal of diabetes. Consequently, appropriate, accurate and fast response detection of glucose has attracted global attention [14, 22]. A variety of instrumental methods are used to detect the blood glucose level [27, 28], but one of the best strategies is the use of electrochemical sensors, which have received more attention thanks to their fast performance and low cost [28, 29]. On the other hand, the use of enzymes in glucose sensors is bounded due to temperature and pH sensitivity as well as high cost [30]. However, compared with them, none-enzymatic electrochemical sensors have received much attention from researchers [30-32].

In this work, we presented an electrochemical detecting platform based on Cu-MOFs nanocomposite modified electrode as a non-enzymatic sensor for sensing of the glucose. In this regard, in order to improve the conductivity and stability of Cu-MOFs film, the MOFs and electrochemically reduced graphene quantum dots (ErGQDs) nanocomposite was prepared on the CCE surface. The constructed modified electrode, Cu-MOFs/ErGQDs/CCE, was used as a sensor for non-enzymatic electrochemical determination of glucose with satisfactory results. Finally, the present sensor was applied to determine the glucose level in human blood serum and saliva samples as the real samples.

Experimental section

Reagents

Benzene-1,3,5-tricarboxylic acid [C_6H_3-1,3,5-$(COOH)_3$](BTC), methyltrimethoxysilane ($C_4H_{12}O_3Si$) (MTMOS), hydrochloric acid, graphite powder, copper (II) chloride, sodium hydroxide, methanol, ethanol and citric acid were purchased from company of Merck (Darmstadt, Germany; www.merckgroup.com). Potassium hexacyanoferrate [$K_3Fe(CN)_6$], uric acid, ascorbic acid, dopamine, potassium chloride, acetaminophen, glucose, potassium nitrate, sodium hydrogen phosphate, and sodium dihydrogen phosphate were purchased from Sigma-Aldrich Chemical company (St. Louis, MO, USA; www.sigmaaldrich.com) with analytical grade. Human serum samples were received from the Blood Transfusion Center (Tabriz, Iran) and saliva samples were collected from healthy volunteers in pathological laboratories.

Electrochemical measurements and instruments

An AUTOLAB PGSTAT-204 (Potentiostat/Galvanostat) with a three-electrode setup; An Ag/AgCl and platinum wire respectively as the reference and auxiliary electrode and Cu-MOFs/ErGQDs nanocomposite modified CCE as the working electrode was utilized for all electrochemical tests including cyclic voltammetric analysis, amperometric analysis and electrochemical impedance spectroscopy. Agilent carry-630 FT-IR spectrometer was utilized for recording of FT-IR spectra to certify the functional groups in the proposed nanocomposites. FT-IR stands for Fourier Transform InfraRed, the preferred method of infrared spectroscopy. In infrared spectroscopy, IR radiation is passed through a sample. Some of the infrared radiation are absorbed by the sample and some of it are passed through (transmitted). The resulting spectrum represents the molecular absorption and transmission, creating molecular fingerprint of the sample. In the present work, FT-IR method was utilized to detect the changes in the preparation of nanocomposites by tracing the changes in functional groups. Scanning electron microscope (SEM) images were taken by Phenom ProX scanning electron microscope equipped with X-ray energy dispersive spectroscopy (EDX) for surface morphological investigation and surface elemental analysis of the modified electrodes, respectively. SEM is an advanced technology used to capture the micro and nanostructure image of the nanomaterials. In SEM, an electron beam focused by electromagnetic lenses scans the surface of prepared materials (in this work, nanocomposites), where the reflected/interacted electrons create an image of the material surface and topography. Energy dispersive x-ray spectroscopy (EDX) is an analytical technique which is used for the identification of compositions of different elements in surface of a specific sample. The EDX analysis can be used to determine the surface elemental composition of individual points or to map out the lateral distribution of elements from the imaged area. X-ray powder diffraction (XRD) is a rapid analytical technique primarily used for phase identification of a crystalline material and can provide information on unit cell dimensions. Here, XRD patterns were obtained by Bruker AXF (D8 Advance) X-ray powder diffractometer in order to crystalline structure analysis of the prepared nanocomposites.

Preparation of the CCE

CCE was composed of graphite powder that is bonded together by a silicate carrier made by sol-gel method. Carbon ceramic electrodes have noticed due to their extensive properties such as no concern for price, easiy manufacturing, porosity and continuous surface renewal. In this work CCE was prepared according to previous methods [33]. Initially 600 µL HCl, 600 µL MTMOS and 900 µL methanol were mixed and gently shaken for 20 min at 40 °C, as soon as the sol-gel mixture get opalescent, 0.3 g of graphite powder was added to it. Then, the product was stirred again to obtain a homogeneous mixture. Finally, the resultant mixture was molded into a Teflon tube and dried at room temperature for 24 hr and used as a working electrode by a copper wire attached to the end.

Synthesis of GQDs

In this work, the production process of GQDs is completed with pyrolysis of citric acid [34]. In order to prepare GQDs in a routine and validated method, 5 g citric acid was put into a 100 mL beaker and heated to 180 ˚C using a heater stirrer under uniform agitation with a magnet. About 10 min later, citric acid molecules are connected to each other and melted, indicated starting pyrolysis reaction [35]. At the same time, the color of the resulted liquid was altered from colorless to light yellow, and then slowly become brown in 40 min, implying the formation of GQDs during the carbonization process [35].

Fabrication of the Cu-MOFs/ErGQDs/CCE

A simple and fast three-step in-situ process was used to fabricate the proposed electrode; Cu-MOFs/ErGQDs/CCE. In this way, at the first step

for the fabrication of Cu-ErGQDs nanocomposite modified CCE, the CCE was immersed in 0.1 M KNO_3 containing CuCl2 (5 mM) and GQDs (500 ppm) solution. A potentiostatic method with fixed potential of -0.55 V for 300 s was utilized for the simultaneous electrodeposition of metallic Cu and ErGQDs on the surface of CCE [12]. Then, the formed electrode; Cu/ErGQDs/CCE, was immersed in 0.1 M KOH solution in order to convert the metallic copper to copper oxide and preparing of the copper oxide-ErGQDs modified electrode (CuO/ErGQDs/CCE) using the cyclic voltammetry technique with 20 cycles in the range of -1.5 to 0.8 V. The following electrochemical reactions show the simultaneous deposition of metallic copper and ErGQDs and the conversion of copper to copper oxide in the presence of KOH, respectively [36].

$Cu^{2+} + 2e^- \rightarrow Cu$ (Eq. 1)

$GQDs + ne^- \rightarrow ErGQDs$ (Eq. 2)

$Cu + OH^- \rightarrow [CuOH + e^-] + OH^- \rightarrow Cu(OH)_2 + e^-$ (Eq. 3)

Or

$2Cu + 2OH^- \rightarrow [Cu_2O + H_2O + 2e^-] + 2OH^- \rightarrow 2CuO^+ H_2O + 2e^-$ (Eq. 4)

In the final step, in order to convert of the CuO or $Cu(OH)_2$ to Cu-MOFs and form the $[Cu_3(BTC)_2]$ on the surface of electrode by in-situ process: the as-deposited CuO/ErGQDs/CCE was immersed into a 50/50 vol% ethanol/water solution containing 5.8 mM BTC and 6.42 mM KNO3 at room temperature. After about 1 min (optimized) placing of the CuO/ErGQDs/CCE in the alcohol/water solution, the color of the electrode surface changes from black to dark blue which indicates the formation of Cu-MOFs on the electrode surface [37, 38].

$3CuO + 2H_3BTC \rightarrow Cu_3(BTC)_2 + 3H_2O$ (Eq. 5)

RESULTS AND DISCUSSION

Electroconversion of the Cu/ErGQDs/CCE to CuO/ErGQDs/CCE

Fig. 1 shows the consecutive cyclic voltammograms (CVs) of the Cu/CCE and Cu/ErGQDs/CCE in the 0.1 M of KOH solution. As can be seen, the resulting CVs in both cases have two obvious oxidation (ipa_1 and ipa_2) and two reduction peaks (ipc_1 and ipc_2), which include the conversion of metallic copper (Cu) to copper oxide (CuO) or copper hydroxide $[Cu(OH)_2]$, that have been reported in previous researches [36, 39]. The results demonstrated that with the increases in the number of scans, the current of all peaks rise. Therefore, it is expected that, the amount of metal

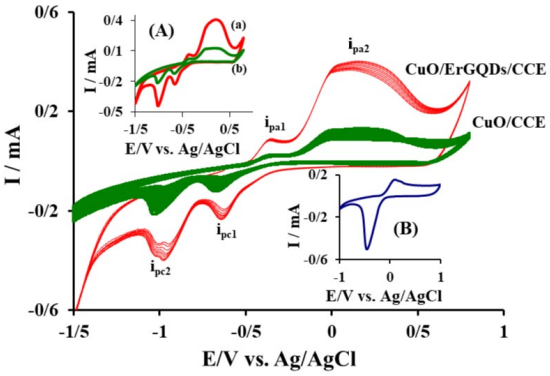

Fig. 1. 25 successive CVs of the CuO/ErGQDs/CCE and CuO/CCE in 0.1 M KOH solution at the scan rate of 50 mV s-1 in the ranges of -1.5 to 0.6 V vs. Ag/AgCl. Inset (A): 1th CV of CuO/ErGQDs/CCE (a) and CuO/CCE (b) in the same conditions. Inset (B): CV of the Cu-MOFs/ErGQDs/CCE in 0.1 M PBS (pH=7.2) at the scan rate of 50 mV s^{-1} in the ranges of -1.0 to 1.0 V vs. Ag/AgCl

copper decrease and turn into the copper oxide or copper hydroxide. According to our previous study [36], it is predicted that in the presented voltammograms, at the first anodic peak (ipa1), metallic copper will first be converted into copper (I) hydroxide (CuOH) or copper oxide (Cu_2O) during the oxidation reaction in the presence of KOH solution. In the second anodic peak (ipa_2), the species produced in the first anodic peak are oxidized to the copper oxide (CuO) or copper hydroxide $[Cu(OH)_2]$. In the reverse scan, the first reduction peak (ipc_1) is expected to include the reduction of the species formed in the most prominent oxidation peak, which is copper oxide, and the hydroxide ion is released. The second reduction peak (ipc_2) is related to other species existing and residual copper oxide species (Eq.1, Eq. 3 and Eq. 4). Inset A in Fig. 1 is related to 1st CVs of CuO/CCE (curve a) and CuO/ErGQDs/CCE (curve b) in 0.1 M KOH solution. It is obvious that, the presence of copper oxide and ErGQDs composite on the surface of the electrode significantly increases the currents of all peaks, which is expected due to the synergistic effect of copper oxide and ErGQDs. Indeed, in the composite, the conductivity, porosity and electron transfer rate increase and subsequently improves the electrocatalytic effect. After conversion of the CuO or $Cu(OH)_2$ to the Cu-MOFs at the surface of CuO/ErGQDs/CCE and construction of the Cu-MOFs/ErGQDs/CCE by in-situ process, its electrochemical behavior was studied in phosphate buffer solution (PBS) (pH=7.2). Inset B shows the CV of the Cu-MOFs/ErGQDs/CCE in 0.1 M PBS (pH=7.2).

Characterization of the Cu-MOFs/ErGQDs/CCE

Morphology of the prepared electrodes was studied by scanning electron microscopy (SEM). Fig. 2 A (low) and B (high) show the SEM images of Cu-MOFs/ErGQDs/CCE with different magnification. According to the observed SEM images, the Cu-MOFs particles have cubic shapes that have been individually deposited on ErGQDs sheets. On the other hand, Cu-MOFs/ErGQDs nanocomposite was formed properly on the surface of CCE with a three-dimensional appropriate structure fabricated which is suitable for the electrocatalytic purposes and mass transfer processes. The surface elemental analysis of the Cu-MOFs/ErGQDs/CCE was performed using energy dispersive X-ray analysis (EDX). The results, depicted as inset in Fig. 1 A, which confirm the presence of C, O, Si, and Cu elements, providing evidence for the successful electrodeposition of the Cu-MOF and ErGQDs on the surface of the CCE. The EDX analysis of the Cu-MOFs/ErGQDs/CCE showed 60.21%, 23.53, 9.14 and 7.12 atomic percentage of C, O, Si and Cu, respectively.

XRD patterns of the Cu-MOFs/CCE (blue line) and Cu-MOFs/ErGQDs/CCE (red line) were illustrated in Fig. 2C, to investigate the crystalline structure of them. The peak at 2θ of 55º in both patterns corresponds to the carbon (006) of the support material (CCE) [40]. ErGQDs display a sharp and weakly broad peak at around 2θ value of 26.5º which shows the formation of similar planes (002) (red line pattern) [41]. The main peaks in the XRD patterns of the Cu-MOFs/ErGQDs/CCE and Cu-MOFs/CCE at 2θ values of 7.02º, 11.6º, 13.76º, 16.11º, 27.01, 20.10º, and 24.71º corresponding to (110), (220), (222), (400), (333), (440), and (040) crystal planes for the Cu-MOFs/ErGQDs/CCE and also Cu-MOFs/CCE. The diffraction peaks were good agreement with those reported in the previous work [42-44], demonstrating a successful synthesis of Cu-MOFs/ErGQDs nanocomposite. On the other hand, Cu-MOFs/ErGQDs/CCE shows sharp and narrowed peaks which point to the products were in high-quality crystalline. These results suggested that the presence of ErGQDs did not affect the formation of the Cu-MOFs crystalline.

FT-IR spectrum can give some information on the functional groups and special bonds present in the Cu-MOFs and Cu-MOFs/ErGQDs nanocomposite (Fig. 2D). The absorption bands of C=O was observed in both spectrums at 1646.17 cm^{-1}. A broad band at 3000-3500 cm^{-1} in each spectrum was assigned to the O-H stretching vibration. The deformation and stretching peak of the O-H group also appeared at 1456.53 cm^{-1}. For MOFs in both spectrums, the C-C stretching and three C-H vibrations on the benzene ring of

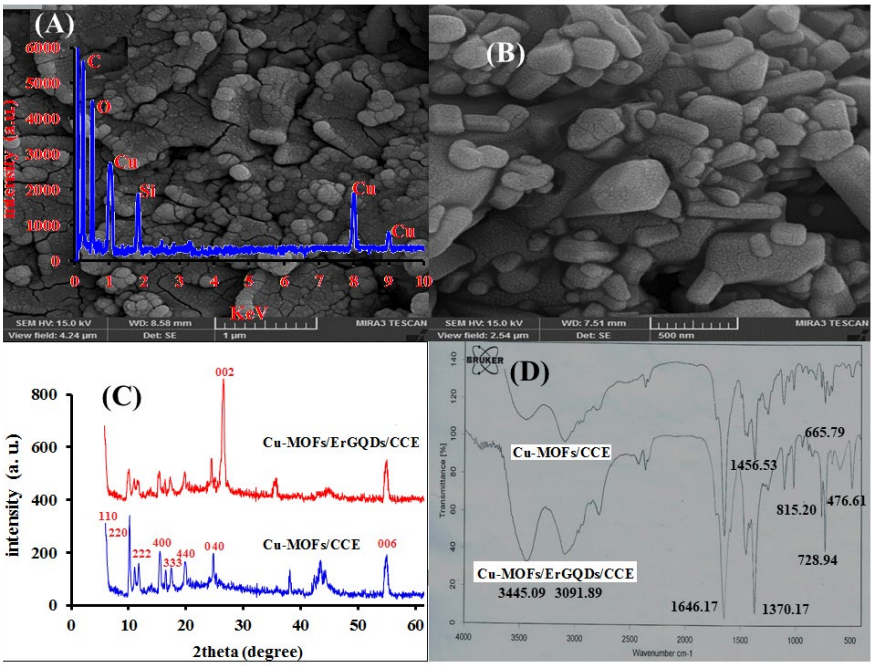

Fig. 2. SEM images of Cu-MOFs/ErGQDs/CCE with different magnification [A (low) and B (high)], (C) XRD patterns of Cu-MOFs/CCE and Cu-MOFs/ErGQDs/CCE. (D) FT-IR spectra of (a): Cu-MOFs/CCE and (b): Cu-MOFs/ErGQDs/CCE. Inset A is the EDX spectrum of the Cu-MOFs/ErGQDs/CCE.

BTC appeared at 665.79, 728.94 and 815.20 cm^{-1} respectively. Also, the sharp peak at 1370.17 cm^{-1} in Cu-MOFs/ErGQDs nanocomposite was related to C-OH that proved proper reduction of GQDs to ErGQDs in the surface of Cu-MOFs/ErGQDs/CCE. The peak at 476.36 cm^{-1} belonged to the stretching vibrations of the Cu-O in the Cu-MOFs and Cu-MOFs/ErGQDs nanocomposite. The FT-IR results are agreed with the reported papers [45-47].

Electrochemical characterization of the Cu-MOFs/ErGQDs/CCE

As presented in Fig. 3, the electrochemical behavior of the Cu-MOFs/ErGQDs/CCE was investigated by cyclic voltammetric method in 0.1 M KCL solution containing a standard redox probe system; $[Fe(CN)_6]^{-3/-4}$ (5 mM). According to the observations, the different electrodes have significant redox peaks with different currents in the presence of $[Fe(CN)_6]^{-3/-4}$, which gradually increases with the modification of the electrode at each stage; MOFs/ErGQDs/CCE (curve d)>Cu-MOFs/CCE(curve c)>ErGQDs/CCE(curve b)>bare CCE(curve a). According to the Fig. 3, it is clear that in the curve d (CV of Cu-MOFs/ErGQDs/CCE), both of the anodic and cathodic peaks increased significantly in compared with other electrodes due to the synergistic effect of Cu-MOFs and ErGQDs. On the other hand, as can be seen in Fig. 3, the peak potential separation (ΔEp) for the Cu-MOFs/ErGQDs/CCE, Cu-MOFs/CCE, ErGQDs/CCE and bare CCE are 0.295 V, 0.478 V, 0.632 V and 0.986 V respectively. The obtained results show

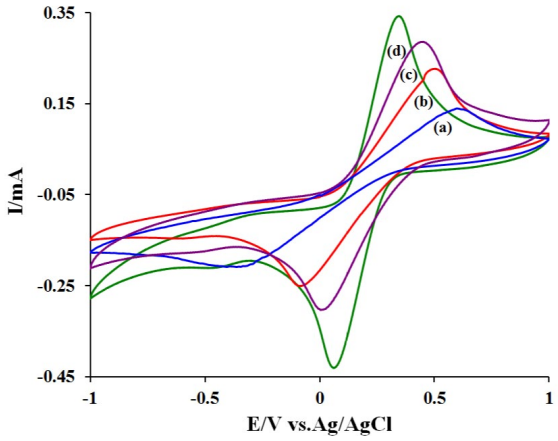

Fig. 3. cyclic voltammograms of (a) CCE, (b) ErGQDs/CCE, (c) Cu-MOFs/CCE, (d) Cu-MOFs/ErGQDs/CCE in 0.1 M KCl containing 5 mM [Fe(CN)6]−3/[Fe(CN)6]−4 as the redox probe at the scan rate of 50 mV s^{-1} in the ranges of -1.0 to 1.0 V vs Ag/AgCl

that the Cu-MOFs/ErGQDs nanocomposite has lower peak potential separation and higher redox peak current than the other electrodes due to the high electron transfer rate, electrical conductivity and the synergistic effect of nanocomposite component.

It is clear that the evaluation of the electrochemical active surface area (ECSA) of the manufactured electrodes is important from the electrochemical point of view, and its purpose is to measure the real surface area of the prepared modified electrode that is in direct contact with the electrolyte solution and charge transfer process. There are different electrochemical methods to estimate the ECSA [48]. One of them is the evaluation of the voltammetric behaviors' of desired electrode in a standard redox probe system such as $[Fe(CN)_6]^{-3}/[Fe(CN)_6]^{-4}$. Here, the redux reaction of $[Fe(CN)_6]^{-3}/[Fe(CN)_6]^{-4}$ on the surface of Cu-MOFs/ErGQDs/CCE is:

$$[Fe(CN)_6]^{-4} \leftrightarrow [Fe(CN)_6]^{-3} + e^- \quad \text{(Eq. 6.)}$$

Since the oxidation of $[Fe(CN)_6]^{-3}/[Fe(CN)_6]^{-4}$ on the surface of the Cu-MOFs/ErGQDs/CCE (curve d in Fig. 3) is a reversible reaction controlled by the diffusion process, therefore the peak current is proportional to the ECSA (A) that can be calculated using the Randles-Sevcik equation (Eq. 7).

$$I_p = 268600\, n^{3/2} A D^{1/2} C\, \upsilon^{1/2} \quad \text{(Eq. 7)}$$

By replacing the relevant values in the Eq. (7), ECSA can be calculated for the Cu-MOFs/ErGQDs/CCE. Where Ip (A), n, A (cm^2), D (cm^2/s), C (mol/cm^3) and υ (V/s) are related to the peak current, number of electrons transferred (n=1), active surface area, diffusion coefficient (7.6×10^{-6} cm^2/s), concentration of the reaction species (5 mM) in the electrolyte and potential scan rate, respectively. The ECSA of the MOFs/ErGQDs/CCE was estimated by anodic peak current of cyclic voltammograms at different scan rate in 5 mM $[Fe(CN)_6]^{3-}/[Fe(CN)_6]^{4-}$ solution as 0.157 cm^2 [49].

To study the future electrochemical characteristics of the prepared electrodes (CCE, ErGQDs/CCE, Cu-MOFs/CCE, Cu-MOFs/ErGQDs/CCE), the ion and charge transfer properties between electrolyte and electrodes, were analyzed by electrochemical impedance spectroscopy (EIS) in 0.1 M NaOH solution at the open circuit potential over a frequency range of 0.01 to 100 KHz. The diameter of the semicircle represents

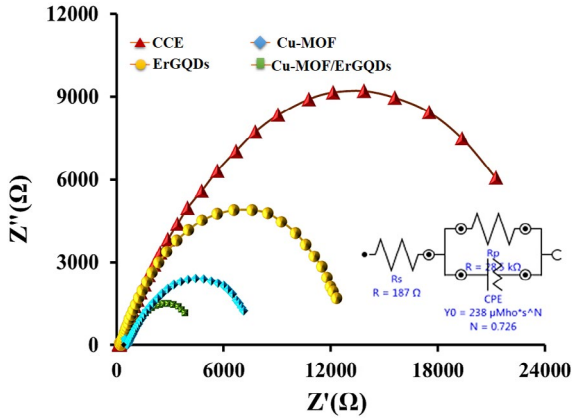

Fig. 4. Nyquist plots of bare CCE, ErGQDs/CCE, Cu-MOFs/CCE and Cu-MOFs/ErGQDs/CCE in 0.1 M NaOH solution from 0.01 to 100,000 Hz. Inset is the corresponding equivalent circuit of the Cu-MOFs/ErGQDs/CCE

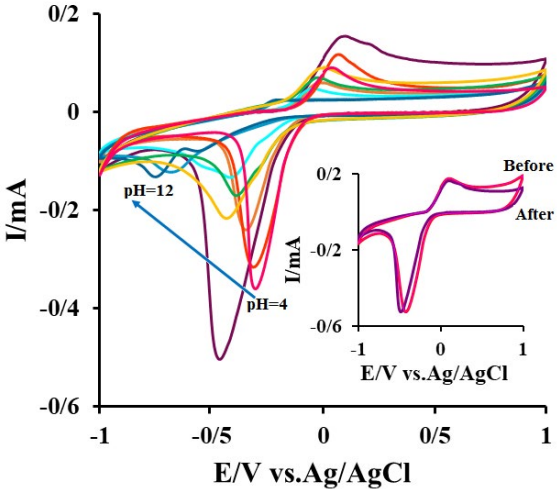

Fig. 5. (A) Cyclic voltammograms of Cu-MOFs/ErGQDs/CCE in different pH in PBS (0.1 M) solution at the scan rate of 50 mV s^{-1} in the ranges of -1.0 to 1.0 V vs Ag/AgCl. Inset: cyclic voltammograms of Cu-MOFs/ErGQDs/CCE in pH=7 (before and after long time working in high basic solution at pH 12)

the Faradic charge-transfer resistance, which normally reflects the electrical conductivity and the electron transfer resistance (Rct) process. As illustrated in Fig. 4, the Rct values of CCE, ErGQDs/CCE, Cu-MOFs/CCE and Cu-MOFs/ErGQDs/CCE are determined as 21.8 and 11.9, 7.8 and 3.9 KΩ, respectively. The observed reduction in resistance is attributed to the enhanced conductivity of these materials. According to the description provided, when ErGQDs and Cu-MOFs particles were deposited individually on the CCE surface, Rct obviously became larger owing to the poor electrical conductivity of them. However, as the integration of ErGQDs and Cu-MOFs, Rct became lower and synergetic effect of the nanocomposite like conductivity, porosity and surface area increased. Thereby, these results indicated that integration of ErGQDs and Cu-MOFs provided more anchoring sites and electrochemical conductivity, thus the electron transfer rate and ion diffusion at the electrode surface was enhanced. Inset shows the corresponding equivalent circuit of Cu-MOFs/ErGQDs/CCE [49, 50].

Effect of pH on the stability of Cu-MOFs/ErGQDs/CCE response

As shown in Fig. 5, the maximum anodic and cathodic peaks of Cu-MOFs/ErGQDs/CCE in the 0.1 M BPS are related to natural pH buffer solution (pH=7). The potential of peaks had been depending on the pH solution and shifted negatively with the increase in the pH of the solution. This indicates the involvement of protons and electrons in the electrochemical reaction at the Cu-MOFs/ErGQDs/CCE. On the other hand, according to inset Fig. 5, the anodic and cathodic peaks of the desired electrode at pH 7 are stable after receiving pH to 12, accomplishing various tests at this pH for a long time and returning the pH to 7, which indicates the stability of the modified electrode and non-destruction of the present modified electrode surface at different pH.

Electrocatalytic activity of the Cu-MOFs/ErGQDs/CCE toward glucose oxidation

The electrocatalytic activity of the Cu-MOFs/ErGQDs/CCE toward electrooxidation of glucose was studied by cyclic voltammetry technique. Fig. 6 A illustrates the cyclic voltammetry results of different electrodes; bare CCE (curve a), Cu-MOFs/CCE (curve b), ErGQDs/CCE (curve c) and Cu-MOFs/ErGQDs/CCE (curve d) in 0.1 M NaOH solution containing 5 mM glucose. It is evident that in all cases except at the bear CCE, in the presence of glucose, the anodic peak current of the electrooxidation of glucose appears, which indicates that, the electrocatalytic activity of the modified electrodes toward glucose oxidation. Actually, as shown in Fig. 6 A, the bare CCE has no specific peak for glucose oxidation, which indicates the poor electrocatalytic effect of bare CCE for the oxidation of glucose (curve a). A broad oxidation peak can be observed in the cyclic voltammogram

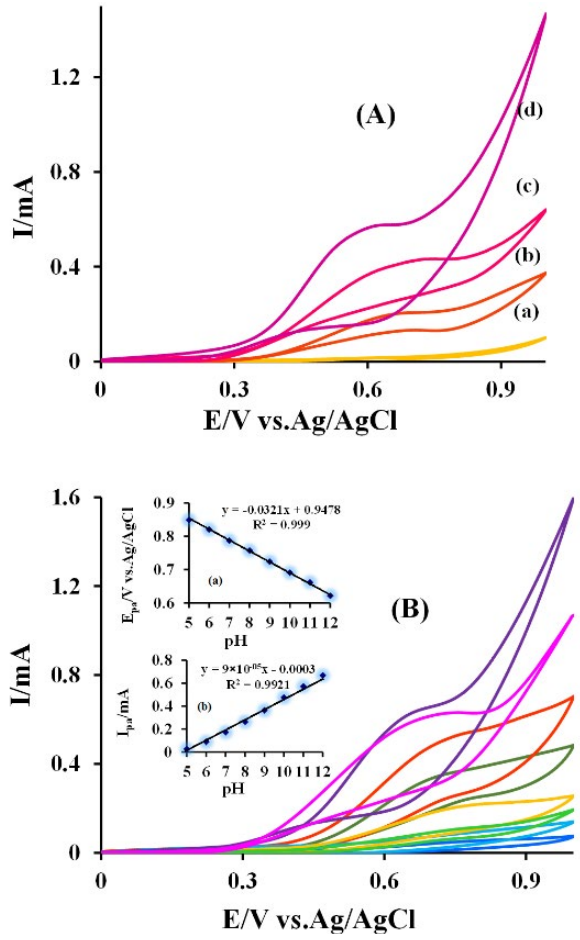

Fig. 6. Cyclic voltammograms of different electrode (a): CCE, (b): ErGQDs/CCE, (c): Cu-MOFs/CCE and (d): Cu-MOFs/ErGQDs/CCE in NaOH 0.1 M containing 5 mM of glucose at scan rate of 50 mV s^{-1} in the ranges of 0.0 to 1.0 V vs Ag/AgCl. (B) cyclic voltammograms of Cu-MOFs/ErGQDs/CCE in PBS (0.1 M) solution at various pH (5.0-12.0) containing 5 mM of glucose at scan rate of 50 mVs^{-1} in the ranges of 0.0 to 1.0 V vs Ag/AgCl. Inset (a) plot of Epa vs. pH and inset (b) plot of Ipa vs. pH

of the ErGQDs/CCE (curve b), with a weak oxidation current signal at high anodic peak potential (Epa) indicates the partial electrocatalytic effect of ErGQDs/CCE toward electrooxidation of glucose.

In the cyclic voltammogram curve of Cu-MOFs/CCE (curve c), a similar oxidation peak with some current signal is appeared, which indicates the increased surface area of the electrode due to its modification by a porous material such as Cu-MOFs.

Nevertheless, compared to the curves of b and c, the Cu-MOFs/ErGQDs/CCE nanocomposite modified electrode (curve d) shows a significant oxidation signal which confirms enhancement of its electrocatalytic effects when ErGQDs and Cu-MOFs are used simultaneously on the surface of electrode [14, 22, 38, 39, 45-47, 51]. It maybe because the high surface area, the porosity of Cu-MOFs and synergistic contributions of these materials that increase the electrocatalytic activity of the Cu-MOFs/ErGQDs/CCE toward glucose oxidation. On the other hand, the synergistic effects of porous Cu-MOFs and ErGQDs causes the improved conduction pathway for electron transfer. Therefore, the Cu-MOFs/ErGQDs/CCE can be used as a glucose-sensing sensor [53-57]. Finally, as can be seen in Fig. 6A, no cathodic peak is observed for the glucose redox system during the reverse scanning, so based on scientific findings, it can be concluded that the electrochemical reaction of glucose molecules on all the present electrodes is totally irreversible [14, 22, 38, 39, 45-47, 51, 53-57].

The effect of pH value on the electrocatalytic activity of the Cu-MOFs/ErGQDs/CCE in the electrooxidation of glucose was investigated. Fig. 6 (B) shows the cyclic voltammograms of Cu-MOFs/ErGQDs/CCE in 5 mM glucose concentration at different pH values (5-12). The results reveal that by increasing the pH values, the anodic and cathodic potential of peaks shift to less positive value [inset (a)] and the peak current increased significantly [inset (b)] which indicates the participation of proton in the glucose oxidation reaction [14, 22, 38, 39, 45-47, 51, 53-57]. As a result, the relationship between the peak potential (Ep) and pH according to the obtained equation Ep (mv) = –0.0321pH + 0.9478 (R^2= 0.999) is linear and corresponds to the Nernstian theoretical slope value of −0.059 V/pH [58]. According to the obtained results and its correlation with the Nernstian equation, the number of protons has been transferred in the process of electrochemical oxidation of glucose, was calculated according to Nernst equation (Eq. 8) [58].

$$E = E^{o} + \left(\frac{RT}{nF}\right) Ln \left(\frac{[Ox]}{[Red]}\right) + \left(\frac{2.303mRT}{nF}\right) pH \qquad \text{(Eq. 8.)}$$

As can be seen in inset b of Fig. 6B, the slope was 32.1 mV pH^{-1} which is almost half of the theoretical value of 59 mv pH^{-1} which shows that, the number of two protons is involved in the electrochemical process of glucose oxidation. [38, 39, 45, 46, 47, 51, 53-57]. Since more reproducible results and high catalytic activity of modified electrode was observed at the pH 12, this pH was used as optimum value for glucose determination in the next measurements.

Fig. 7 demonstrated the cyclic voltammograms of the Cu-MOFs/ErGQDs/CCE in different concentrations of glucose and calibration curve of the oxidation peak current vs. concertation of glucose as the inset. As can be seen, there is a linear relationship between the glucose concentration and oxidation peak current at the Cu-MOFs/ErGQDs/CCE by cyclic voltammograms curves in the ranges of glucose concentrations (1-5 mM). The peak current of Cu-MOFs/ErGQDs/ CCE was linear for glucose concentration with linear correlation (R^2=0.9991). The linearequation was

I_{pa}(mA)= 8×10^{-6} C(mM) + 0.0002, where Ipa is the peak current and C is the glucose concentration. The effective response to elevated glucose concentration indicates that the Cu-MOFs/ ErGQDs/CCE could be considered as an effective electrocatalyst for glucose oxidation and electrodetermination [38, 39, 45-47, 51, 53-60].

In order to determine the electrochemical reaction kinetics of glucose, the effect of potential scan rate on the electrooxidation reaction of glucose in various scan rates from 5 to 100 mV s^{-1} was investigated in a 0.1 M NaOH solution containing 5 mM glucose by cyclic voltammetric technique and the obtained results are shown in Fig. 8. As can be seen, the anodic peak current (Ipa) increases accordingly with the increasing of the scan rate from 5 to 100 mV s^{-1}. The plot of Ipa vs. $\upsilon^{1/2}$ displays a linear dependency with a correlation coefficient of 0.9979 which can be observed in inset, suggesting the electrochemical oxidation of glucose at the Cu-MOFs/ErGQDs/CCE is a diffusion-controlled process [45-47, 51, 53-63].

Furthermore, based on the theory of Laviron for an irreversible electrode process, the E-Log υ plot (Fig. 8) can be used for the estimating of charge transfer coefficient (α) and catalytic rate constant (k_s) based on the equation 9.

$$E_p = E^{\circ\prime} + \left(\frac{2.303RT}{\alpha nF}\right)\log\left(\frac{RTk_s}{\alpha nF}\right) + \left(\frac{2.303RT}{\alpha nF}\right)\log \upsilon \qquad \text{(Eq. 9)}$$

where n, F, R, T, and other symbols have their conventional and usual meanings [50]. By using the Laviron equation, the α and Ks were calculated from the result of Fig. 8 and its inset as about 0.5 and 3.24 $M^{-1}s^{-1}$, respectively.

Amperometric sensing of glucose by the Cu-MOFs/ ErGQDs/CCE

Under the optimal conditions mentioned above, a glucose sensing platform was constructed based on the high-quality electrocatalytic activity of Cu-MOFs/ErGQDs/CCE toward the oxidation

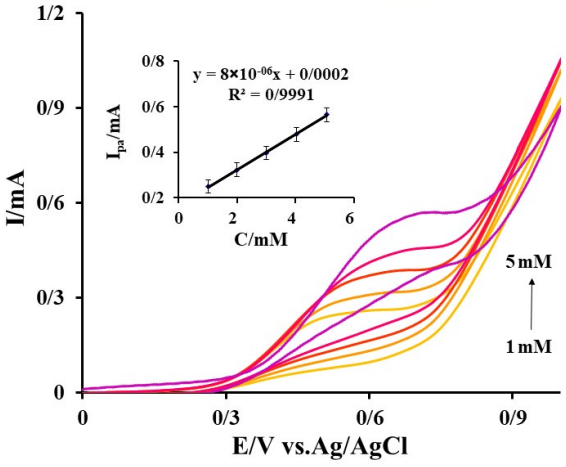

Fig. 7. Cyclic voltammograms of Cu-MOFs/ErGQDs/CCE in 0.1 M NaOH solution containing different concentration of glucose 1- 5 mM at scan rate of 50 mVs^{-1} in the ranges of 0.1 to 1.0 V vs Ag/AgCl. Inset shows the calibration curve

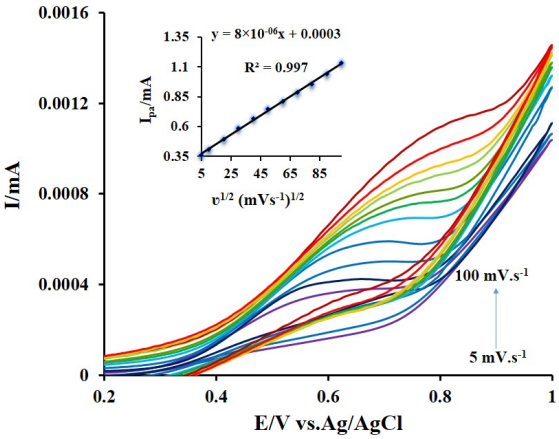

Fig. 8. Cyclic voltammograms of the Cu-MOFs/ErGQDs/CCE in 0.1 M NaOH solution in the + 5 mM glucose and the potential window of 0.2 V to +1.0 V at different scan rates of 5-100 mV s^{-1}. Inset: plot of Epa vs. Log υ

of glucose. The analytical performance of the glucose sensing platform was investigated using amperometric technique. Fig. 9 describes the amperometric responses of the Cu-MOFs/ErGQDs/CCE at 0.6 V after successive addition of glucose in 0.1 M NaOH while stirring solution. It can be observed, when glucose is added, the current-time curve sensitively exhibits apparent current step, which refers to the fast response of Cu-MOFs/ErGQDs/CCE. As shown in Fig. 9, the response current increases linearly with increasing glucose concentration over the ranges of 2-70 µM (Fig. 9A and inset) and 50-500 µM (Fig. 9B and inset), with good correlations (R^2 = 0.9935 and 0.9966) (insets), respectively. Moreover, the detection limit of this sensing platform was estimated as 0.59 µM (S/N = 3), while the sensitivity in the lower concentration range was calculated as 5069 µA mM^{-1} cm^{-2}. To further evaluate the analytical performance of our proposed glucose-sensing platform, the comparison of our work with other reported glucose sensors was performed and shown in Table 1. As shown in Table 1, a comparison was done with the reported glucose sensors. The wide

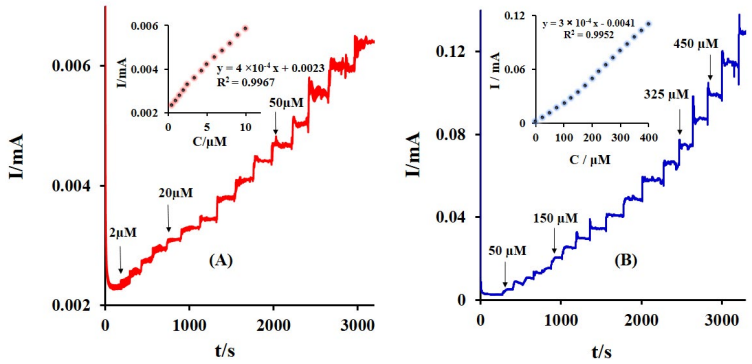

Fig. 9. Amperometric i-t curve for the determination of glucose at the Cu MOFs/ErGQDs/CCE in 0.1 M NaOH solution with an applied potential of 0.6 V. (A) 2-70 µM of glucose and (B) 50-500 µM of glucose. Insets are the calibration curves

Table 1. Comparison of fabricated non-enzymatic glucose sensor with others reported amperometric-sensing platform

Electrode materials	Linear range (µM)	Detection limit (µM)	Sensitivity (µA.mM^{-1}.cm^{-2})	Ref.
Cu-MOF	0.5-5000	0.07	-	47
Ni(TPA)-SWCNT/GCE	20-4400	4.6	-	51
C-Ni-MOF-74/G/GCE	5-1400	0.44	7234	53
NiP/CCE	0.5-5000	0.1	40	54
graphene@ZIF-67	1-805.5	0.36	1521.1	56
Cu-MOF/MWNTs/GCE	0.5-118400	0.4	3878	57
CoCu oxides/CF	1-1070	0.72	11.916	60
Ni@Cu-MOF	5-2500	1.67	1703.33	61
CuONPs/Ce-MOF	0.005-8600	0.002	2058.5	62
Co_3O_4-MCNT/GCE	1.0-122	0.28	2550	63
NiNPs/SMWNTs	1-1000	0.5	1438	64
Au@Cu_2O	50-2000	18	715	65
CC@MOF-74(NiO) @NiCo LDH	10-9000	0.278	1699	66
Ni-MOF/Ni/NiO/C	4–5664	0.8	367.45	67
Pt/PANI/rGO/CuO	0-13000	1.5	1252	68
Co_3(BTC)$_2$MOFs/GCE	1-1380	0.33	1792	69
Co-MOF	5-900	1.6	169	70
PA-ZIF-67@GS	0.025-1257.75	0.086	2718.3	71
Au NPs-TiO_2/PANI	10-10000	0.15	379.8	72
Ni-MoS_2/rGO	5-8200	2.7	256.6	73
ZnO/Co_3O_4/rGO	15-10000	0.043	1551.38	74
Cu-MOF/ErGQD/CCE	2-500	0.59	5069	This work

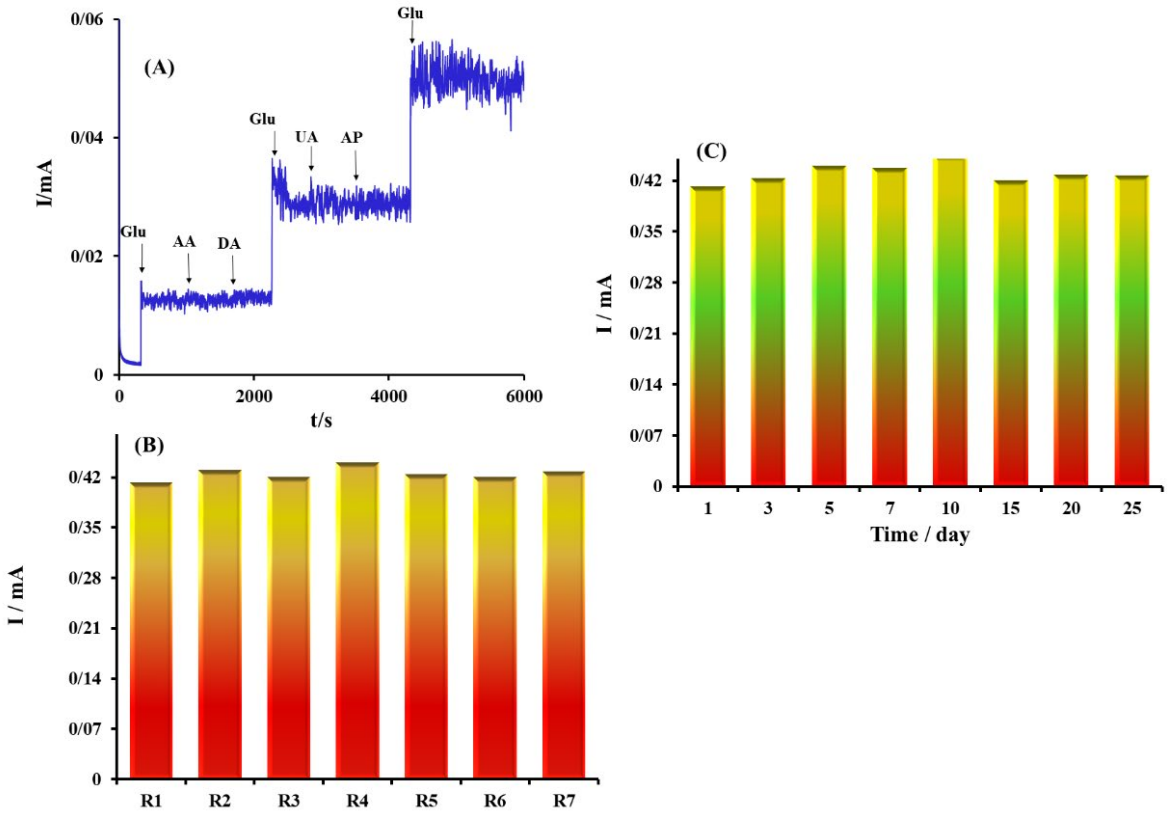

Fig. 10. Amperometric responses of Cu-MOFs/ErGQDs/CCE to successive addition of glucose, ascorbic acid (AA), dopamine (DA), glucose, uric acid (UA), acetaminophen (AP) and glucose for selectivity of Cu-MOFs/ErGQDs/CCE in stirred 0.1 M NaOH solution with an applied potential of 0.6 V. (B) The reproducibility investigation of seven successive experiments (R1–R7) for determination of 5 mM glucose in 0.1 M NaOH solution with an applied potential of 0.6 V and (C) The storage stability of the modified electrode for determination of 5 mM glucose 0.1 M NaOH solution with an applied potential of 0.6 V vs time (day).

sensitivity, anticipated LOD values, suppression of other electrodes, fabrication simplicity, and suitability for further research were all significant reasons in favor of the proposed electrode. Overall, it can be concluded that, our proposed sensing platform performs reasonably well.

Selectivity, reproducibility and stability of glucose sensor

The selectivity or anti-interference performance of physiological substances in real samples is a crucial consideration in the implementation of electrochemical sensors. Numerous studies have demonstrated that there are several substances present in biological samples, including fructose, lactose, ascorbic acid, dopamine, KCl, and NaCl, which exhibit similar electrochemical behaviors to glucose [66, 71-74]. Consequently, the accurate detection of glucose can be hindered by the interference caused by these substances. Hence, it is of utmost importance to effectively eliminate the interference of these factors in order to ensure accurate glucose detection. For glucose determination, the interference of several physiological coexisting materials such as ascorbic acid (AA), dopamine (DA), uric acid (UA), and acetaminophen (AP) were estimated using the amperometric i-t curve in a homogeneous solution of 0.1 M NaOH (Fig. 10A). The initial current response was associated with the addition of 10 µM glucose. Furthermore, the current response has no apparent signal with the addition of a 10-fold excess of interference species, by successfully addition of the second 10 µM glucose, again an analogous grow with the previous steps was observed in the current response. Therefore, it can be concluded that Cu-MOFs/ErGQDs/CCE showed acceptable anti-interference performance and excellent stability performance and a high selectivity behavior in glucose detection.

The reproducibility of the proposed sensors was investigated by recording the glucose oxidation current response for five independently selected

Table 2. Results of the recovery test of glucose in real samples (n=3)

Sample	Concentration (μM)	Expected (μM)	Found (μM)	Recovery (%)	R.S.D. (%)
Human blood serum	0.0	0.0	200.0	-	-
	40.0	240.0	255.7	106.5	2.98
	100.0	300.0	292.2	97.4	3.10
	150.0	350.0	346.9	99.1	3.61
Saliva	0.0	0.0	80.0	-	-
	40.0	120.0	119.5	99.6	2.58
	60.0	140.0	136.8	97.7	2.95
	80.0	160.0	160.8	100.3	3.52

Cu-MOFs/ErGQDs/CCE provided by the same procedures in 0.1 M NaOH solution containing 5 mM of glucose through consecutive experiments. The relative standard deviation (RSD) of their anode peak current is only 2.09 %, indicating that the electrodes have a good reproducibility (Fig. 10B).

In addition, the storage life or long-term stability of the proposed sensor was evaluated by detecting the electrochemical signals of glucose at a fixed concentration and over a long period using the amperometric technique. Measured currents over 25 days shows a stable current response (Fig. 10 C) (maintaining 96.97% of the initial signal) indicating that the proposed sensor has good stability.

Real sample analysis

To verify the practical efficiency of the detection platform, human blood serum and saliva samples were analyzed for glucose detection. Human blood serum were obtained from the Blood Transfusion Center of Tabriz, Iran and saliva samples were collected from healthy volunteers. To facilitate glucose detection in the human blood serum, the serum samples underwent centrifugation at a speed of 8000 rpm for a duration of 15 min. Subsequently, the supernatant was gathered to enable the electrochemical measurement of glucose levels using the standard addition method. To collect the saliva samples, first, the oral cavity was completely washed, then the saliva samples were collected from volunteers in a vial and stored at 4 °C before the assay. The saliva samples were used directly without any purification before measurements. For glucose sensing with Cu-MOFs/ErGQDs/CCE, amperometric i-t curves were recorded for diluted human blood serum and saliva samples with standard addition technique. The recovery is defined as following equation (Eq. 10) [59]:

$$\text{Recovery\%} = (C_{found} - C_{real}/C_{added}) \times 100 \quad \text{(Eq. 10)}$$

Where Cfound is the concentration of analyte which was detected by Cu-MOFs/ErGQDs/CCE, Creal is the concentration of glucose in real samples and Cadded is the concentration of glucose was spike in the real samples. The results are presented in Table 2. This table shows good recovery with average of about 101% and 99.2% for glucose detection in human blood serum and saliva samples, respectively. The results suggest that the developed glucose sensor can be successfully utilized for glucose detection in real samples.

CONCLUSION

In this study, a novel and fast response platform based on in-situ synthesis of Cu-metal organic frameworks (Cu-MOFs) integrated with electrochemically reduced graphene quantum dots (ErGQDs) was developed through electrochemical deposition method and conversation process for non-enzymatic glucose determination. In this regard, in the first step, the Cu metal and ErGQDs simultaneously electrodeposited on the surface of CCE. Then, the metallic copper was converted to copper oxide; CuO/ErGQDs/CCE, via cyclic voltammetric technique. Finally, CuO on/in the CuO/ErGQDs/CCE easily transformed to MOFs through the in-situ conversation and preparation of the Cu-MOFs/ErGQDs/CCE. Then, the Cu-MOFs/ErGQDs/CCE was used as an electrocatalyst toward the oxidation of glucose. The Cu-MOFs/ErGQDs/CCE, exhibited high electrocatalytic activity, good stability, reproducibility and selectivity in glucose detection. The prepared sensor offered a wide detection range (from 2 to 500 μM) with a low detection limit of 0.59

μM (S/N = 3) and high sensitivity (5069 μA mM^{-1} cm-2). Finally, the Cu-MOFs/ErGQDs/CCE with satisfactory results was utilized to detect the glucose in real samples (human blood serum and saliva samples) demonstrate the excellent sensing performance of the present sensor. Therefore, it can be suggesting that the developed sensor may become a promising simple tool for the detection of glucose in biological samples.

ACKNOWLEDGMENTS

The authors gratefully acknowledge the Research Council of Azarbaijan Shahid Madani University for financial support.

FUNDING

The author(s) received no financial support for the research, authorship, and/or publication of this article.

CONFLICT OF INTEREST

The authors declare no conflict of interest.

REFERENCES

1. Hu Z, Zhao D. Metal-organic frameworks with Lewis acidity: synthesis, characterization, and catalytic applications. CrystEngComm. 2017; 19(29): 4066-4081.
2. Kempahanumakkagari S, Kumar V, Samaddar P, Kumar P, Ramakrishnappa T, Kim KH. Biomolecule-embedded metal-organic frameworks as an innovative sensing platform. Biotechnol. Adv. 2018; 36(2): 467-481.
3. Xu Y, Li Q, Xue H, Pang H. Metal-organic frameworks for direct electrochemical applications. Coord. Chem. Rev. 2018; 376: 292-318.
4. Yoo Y, Jeong HK. Rapid fabrication of metal organic framework thin films using microwave-induced thermal deposition. ChemComm. 2008; 36(21): 241-244.
5. Rodenas T, Luz I, Prieto G, Seoane B, Miro H, Corma A, Kapteijn F, Xamena FXLi, Gascon J. Metal-organic framework nanosheets in polymer composite materials for gas separation. Nat. Mater. 2015; 14: 48-55.
6. Falcaro P, Hill AJ, Nairn KM, Jasieniak J, Mardel JI, TJ Bastow, Mayo SC, Gimona M, Gomez D, Whitfield HJ, Riccò R, Patelli A, Marmiroli B, Amenitsch H, Colson T, Villanova L, Buso D. A new method to position and functionalize metal-organic framework crystals. Nat. Commun. 2011; 2 (237): 237-234.
7. Makiura R, Motoyama S, Umemura Y, Yamanaka H, Sakata O, Kitagawa H. Surface nano-architecture of a metal-organic framework. Nat. Mater. 2010; 9(7): 565-571.
8. Li M, Dincă M. Reductive Electrosynthesis of Crystalline Metal-Organic Frameworks. J. Am. Chem. Soc. 2011; 133(33): 12926-12929.
9. Habibi B, Pashazadeh A, Pashazadeh S, Saghatforoush LA. Copper/zeolitic imidazolate framework-8 integrated by boron nitride as an electrocatalyst at the glassy carbon electrode to sensing of the clopidogrel. J. Solid State Chem. 2023; 323: 123982.
10. Qi Y, Lin S, Chen C, Liu Y, Qiao Z, Kuang X, Suiang Q, chao HY. Increased proton conductivity of metal-organic framework micro-film prepared by a facile salt-free approach. J. Mater. Chem. A. 2014; 2 (23): 8849-8853.
11. Guo H, Zhu G, Hewitt IJ, Qiu S. "Twin Copper Source" Growth of Metal-Organic Framework Membrane: Cu3 (BTC) 2 with High Permeability and Selectivity for Recycling H2. J. Am. Chem. Soc. 2009; 131 (5): 1646-1647.
12. Chen YC, Chiang WH**,** Kurniawan D, Yeh PC, Otake KI, Kung CW. Impregnation of Graphene Quantum Dots into a Metal−Organic Framework to Render Increased Electrical Conductivity and Activity for Electrochemical Sensing. ACS Appl. Mater. Interfaces. 2019; 11(38): 35319-35326.
13. Habibi B, Pashazadeh A, Pashazadeh S, Saghatforoush LA. Electrocatalytic oxidation and determination of hydrazine in alkaline medium through in situ conversion thin film nanostructured modified carbon ceramic electrode. J. Electroanal. Chem. 2022; 907 (2): 116038.
14. Rahmani K, Habibi B. Electrofabrication of the Ternary NiCuFe Alloy Nanoparticles/ERGO Nanocomposite: Effective Electrooxidation of the Glucose and Glycerol in Alkaline Media. Chemistryselect. 2020; 5 (26): 7990-8001.
15. Altegani S, Naser E, Badmus KO, Khotseng L. Synthesis, Properties, and Applications of Metal Organic Frameworks Supported on Graphene Oxide. *Coat.* 2023; *13* (8): 1456.
16. Habibi B, Pashazadeh S. Fabrication, characterization and performance evaluation of an amplified electrochemical sensor based on MOFs nanocomposite for leukemia drug Imatinib determination. Sens. Bio-Sens. Res. 2023; 42: 100604.
17. Habibi B, Pashazadeh S, Pashazadeh A, Saghatforoush, LA. An amplified electrochemical sensor employing one-step synthesized nickel-copper-zinc ferrite/carboxymethyl cellulose/graphene oxide nanosheets composite for sensitive analysis of omeprazole. RSC Adv. 2023; 13 (43): 29931-29943.
18. Habibi B, Pashazadeh A, Saghatforoush LA. Zn-mesoporous metal-organic framework incorporated with copper ions modified glassy carbon electrode: Electrocatalytic oxidation and determination of amoxicillin. Microchem. J. 2021; 164*:*106011.
19. Wei D, Tang W, Gan Y, Xu X. Graphene quantum dot-sensitized Zn-MOFs for efficient visible-light-driven carbon dioxide reduction. Catal. Sci. Technol. 2020; 10(16): 5666-5676.
20. Bacon M, Bradley SJ, Nann T. Graphene Quantum Dots. Part Part Syst Charact. 2014; 31 (4): 415-428.
21. Sheikh Mohd Ghazali SAI, Is F, Zamil ZN, Zulkifli NN, Adam N. "Graphene quantum dots: A comprehensive overview. Chemistry Open. 2023; 21 (1):0285.
22. Li M, Liu C, Qi L**,** Liu H. Nitrogen-Doped Graphene Quantum Dots Anchored on Hollow Zeolitic Imidazolate Framework8 Colloidosomes for Fluorescence Detection of Glucose. "ACS Appl. Nano Mater." 2022; 5 (4): 5425-5438.
23. Ahirwar S, Mallick S, Bahadur D. Electrochemical Method To Prepare Graphene Quantum Dots and Graphene Oxide Quantum Dots. ACS Omega. 2017; 2 (11): 8343-8353.
24. Kaur A, Kaur A, Pandey K, Kaur R, Vashishat N , Kaur M. Nanocomposites of Carbon Quantum Dots and Graphene Quantum Dots: Environmental Applications as Sensors. Chemosensors 2022; 10 (9): 367.
25. Chen YC, Chiang WH**,** Kurniawan D, Yeh PC, Otake KI, Kung CW. Impregnation of Graphene Quantum Dots into a Metal-Organic Framework to Render Increased Electrical Conductivity and Activity for Electrochemical Sensing. ACS Appl. Mater. Interfaces. 2019; 11 (38): 35319-35326.
26. Deshpande AD, Harris-Hayes M, Schootman M.

Epidemiology of diabetes and diabetes-related complications. PT. 2008; 88(11): 1254-1264.
27. Steiner MS, Duerkop A, Wolfbeis OS. Optical methods for sensing glucose. Chem. Soc. Rev. 2011; 40 (9): 4805-4839.
28. Chen C, Xie Q, Yang D, Xiao H, Fu Y, Tan Y, Yao S. Recent advances in electrochemical glucose biosensors: a review. RSC Adv. 2013; **3** (14): 4473-4491.
29. Li J, Hu H, Li H, Yao C. Recent developments in electrochemical sensors based on nanomaterials for determining glucose and its byproduct H2O2. J. Mater. Sci. 2017; 52 (17): 10455-10469.
30. Hassan MH, Vyas C, Grieve B, Bartolo P. Recent advances in enzymatic and non-enzymatic electrochemical glucose sensing. Sens. 2021; 21(14): 4672.
31. Wang G, He X, Wang L, Gu A, Huang Y, Fang B, Geng B, Zhang. Non-enzymatic electrochemical sensing of glucose. Microchim. Acta. 2013; 180: 161-186.
32. Wei M, Qiao Y, Zhao H, Liang J, Li T, Luo Y, Lu S, Shi X, Lu W, Sun X. Electrochemical non-enzymatic glucose sensors: recent progress and perspectives. Chem comm. 2020; 56 (93): 14553-14569.
33. Habibi B, Haghighi SY. Electrosynthesized Reduced Graphene Oxide-Supported Platinum, Platinum-Copper and Platinum-Nickel Nanoparticles on Carbon-Ceramic Electrode for Electrocatalytic Oxidation of Ethanol in Acidic Media. IJCCE. 2019; 38 (3): 167-181.
34. Dong Y, Shao J, Chen C, Li H, Wang R, Chi Y, Lin X, Chen G. Blue luminescent graphene quantum dots and graphene oxide prepared by tuning the carbonization degree of citric acid. Carbon. 2012; 50 (12): 4738-4743.
35. Alizadeh T, shokri M. A new humidity sensor based upon graphene quantum dots prepared via carbonization of citric acid. Sens. Actuators B Chem. 2016; 222: 728-734.
36. Mohammad Rezaei R, Abbas Zadeh J, Golmohammadpour M, Hosseinzadeh E. Simultaneous electrodeposition of reduced graphene quantum dots/copper oxide nanocomposite on the surface of carbon ceramic electrode for the electroanalysis of Adenine and Guanine. Electroanalysis. 2021; 33 (12): 2428-2436.
37. Zeng Y, Camarada ME, Lu X, Tang K, Li W, Qiu D, Wen Y, Wu G, Luo Q, Bai L. Detection and electrocatalytic mechanism of zearalenone using nanohybrid sensor based on copper-based metal-organic framework/magnetic Fe3O4-graphene oxide modified electrode. Food Chem. 2022; 370: 131024.
38. Caddeo F, Vogt R, Weil D, Sigle W, Toimil Molares ME**,** Maijenburg AW. Tuning the Size and Shape of Nano MOFs via Templated Electrodeposition and Subsequent Electrochemical Oxidation. ACS Appl. Mater. Interfaces. 2019; 11 (28): 25378-25387.
39. Giri SD, Sarkar A. Electrochemical Study of Bulk and Monolayer Copper in Alkaline Solution. J. Electrochem. Soc. 2016; 163 (3): 52-59.
40. Habibi B, Delnavaz N. Electrooxidation of glycerol on nickel and nickel alloy (Ni–Cu and Ni–Co) nanoparticles in alkaline media. RSC Adv. 2016; 6(38): 31797-31806.
41. Muthurasu A, Dhandapani P, Ganesh V. Facile and simultaneous synthesis of graphene quantum dots and reduced graphene oxide for bio-imaging and supercapacitor applications. New J Chem. 2016; 40(11): 9111-9124.
42. Liu S, Sun L, Xu F, Zhang J, Jiao C, Li F, Li Z, Wang S, Wang Z, Jiang X, Zhou H, Yang l, Schick C. Nanosized Cu-MOFs induced by graphene oxide and enhanced gas storage capacity. Energy Environ Sci. 2013; 6(3): 818-823.
43. Lee DY, Shinde DV, Yoon SJ, Cho KN, Lee W, Shrestha NK, Han SH. Cu-based metal–organic frameworks for photovoltaic application. J Phys Chem C. 2014; 118(30): 16328-16334.
44. Gascon J, Aguado S, Kapteijn F. Manufacture of dense coatings of Cu3(BTC)2 (HKUST-1) on α-alumina. Microporous Mesoporous Mater. 2008; 113(1-3): 132-138.
45. Moradi Golsheikh A, Yeap GY, Yam FK, San Lim H. Facile fabrication and enhanced properties of copper-based metal organic framework incorporated with graphene for non-enzymatic detection of hydrogen peroxide. Synth Met. 2020; 260: 116272.
46. Chen S, Wang C, Zhang M, Zhang W, Qi J, Sun X, Wang L, Li J. N-doped Cu-MOFs for efficient electrochemical determination of dopamine and sulfanilamide. J Hazard. Mater. 2020; 390: 122157.
47. Arul P, John SA. Electrodeposition of CuO from Cu-MOF on glassy carbon electrode: A non-enzymatic sensor for glucose. J Electroanal Chem. 2017; 799: 61-69.
48. Lukaszewski M, Soszko M, Czerwiński A. Electrochemical methods of real surface area determination of noble metal electrodes–an overview. Int J Electrochem. Sci, 2016; 11(6): 4442-4469.
49. Habibi B, Pashazadeh S, Saghatforoush LA, Pashazadeh A. Direct electrochemical synthesis of the copper based metal-organic framework on/in the heteroatoms doped graphene/pencil graphite electrode: Highly sensitive and selective electrochemical sensor for sertraline hydrochloride. J Electroanal Chem. 2021; 888: 115210.
50. Iftikhar T, Xu Y, Aziz A, Ashraf G, Li G, Asif M, Xiao F, Liu H. Tuning Electrocatalytic Aptitude by Incorporating α-MnO_2 Nanorods in Cu-MOF/rGO/CuO Hybrids: Electrochemical Sensing of Resorcinol for Practical Applications. ACS Appl Mater.Interfaces. 2021; 13 (27): 31462-31473.
51. Wanga F, Chen X, Chen L, Yang J, Wang Q. High-performance non-enzymatic glucose sensor by hierarchical flower-like nickel (II)-based MOF/carbon nanotubes composite. Mater Sci Eng C. 2019; 96: 41-50.
52. Handa Y, Watanabe K, Chihara K, Katsuno E, Horiba T, Inoue M, Komaba S. The Mechanism of Electro-Catalytic Oxidation of Glucose on Manganese Dioxide Electrode Used for Amperometric Glucose Detection. J Electrochem Soc. 2018; 165 (11): 742-749.
53. Zhang Y, Xu J, Xia J, Zhang F, Wang Z. MOF-Derived Porous Ni2P/Graphene Composites with Enhanced Electrochemical Properties for Sensitive Nonenzymatic Glucose Sensing. ACS Appl Mater Interfaces. 2018; 10 (45): 39151-39160.
54. Salimi A, Roushani M. Non-enzymatic glucose detection free of ascorbic acid interference using nickel powder and nafion sol-gel dispersed renewable carbon ceramic electrode. Electrochem Commun. 2005; 7 (9): 879-887.
55. Liu B, Wang X, Liu H, Zhai Y, Li L, Wen H. 2D MOF with electrochemical exfoliated graphene for nonenzymatic glucose sensing: Central metal sites and oxidation potentials. Anal Chim Acta. 2020; 1122: 9-19.
56. Chen X, Liu D, Cao G, Tang Y, Wu C. In Situ Synthesis of a Sandwich-like Graphene@ZIF-67 Heterostructure for Highly Sensitive Nonenzymatic Glucose Sensing in Human Serums. ACS Appl Mater Interfaces. 2019; 11 (9): 9374-9384.
57. Wu L, Lu Z, Ye J. Enzyme-free glucose sensor based on layer-by-layer electrodeposition of multilayer films of multi-walled carbon nanotubes and Cu-based metal framework modified glassy carbon electrode. Biosens Bioelectron. 2019; 135: 45-49.
58. Bard AJ, Faulkner LR. Electrochemical Methods: Fundamentals

and Applications. 2nd ed. Ed. or Eds. Wiley; 2001.
59. Khosroshahi Z, Karimzadeh F, Kharazia M, Allafchian A. A non-enzymatic sensor based on three-dimensional graphene foam decorated with Cu-xCu2O nanoparticles for electrochemical detection of glucose and its application in human serum. Mater Sci Eng C. 2020; 108: 110216.
60. Wei C, Li X, Xiang W, Yu Z, Liu Q. MOF derived seaweed-like CoCu oxides nanorod arrays for electrochemical non-enzymatic glucose sensing with ultrahigh sensitivity. Sens. Actuators: B. Chem. 2020; 324: 128773.
61. Xu Z, Jia L, Zhu RR, Du L, Zhao QH. High-performance non-enzymatic glucose electrochemical sensor constructed by transition nickel modified Ni@Cu-MOF. J Electroanal Chem. 2020; 858: 113783.
62. Zhang J, Chen L, Yang K. In situ synthesis of CuO nanoparticles decorated hierarchical Ce-metal-organic framework nanocomposite for an ultrasensitive non-enzymatic glucose sensor. Ionics. 2019; 25 (26): 4447-4457.
63. Wei C, Li X, Xiang W, Yu Z, Liu Q. MOF derived seaweed-like CoCu oxides nanorod arrays for electrochemical non-enzymatic glucose sensing with ultrahigh sensitivity. Sens. Actuators B Chem. 2020;324:128773.
64. Nie H, Yao Z, Zhou X, Yang Z, Huang S. Nonenzymatic electrochemical detection of glucose using well-distributed nickel nanoparticles on straight multi-walled carbon nanotubes. Biosens Bioelectron. 2011; 30(1):28-34.
65. Su Y, Guo H, Wang Z, Long Y, Li W, Tu Y. Au@ Cu_2O core-shell structure for high sensitive non-enzymatic glucose sensor. Sens. Actuators B Chem. 2018; 255: 2510-2519.
66. Wang L, Yang Y, Wang B, Duan C, Li J, Zheng L, Li J, Yin Z. Bifunctional three-dimensional self-supporting multistage structure CC@ MOF-74 (NiO)@ NiCo LDH electrode for supercapacitors and non-enzymatic glucose sensors. J Alloys Compd. 2021; 885:160899.
67. Liu Y, Tu D, Zheng W, Lu L. You W, Zhou S, Huang P, Li R, Chen X. A strategy for accurate detection of glucose in human serum and whole blood based on an upconversion nanoparticles-polydopamine nanosystem. Nano Res. 2018; 11(6): 3164-3174.
68. Fang L, Zhu Q, Cai Y, Liang B, Ye X. 3D porous structured polyaniline/reduced graphene oxide/copper oxide decorated electrode for high performance nonenzymatic glucose detection. J Electroanal Chem. 2019; 841:1-9.
69. Shahrokhian S, Ezzati M, Hosseini H. Fabrication of a sensitive and fast response electrochemical glucose sensing platform based on co-based metal-organic frameworks obtained from rapid in situ conversion of electrodeposited cobalt hydroxide intermediates. Talanta. 2020; 210:120696.
70. Zhang L, Wang N, Cao P, Lin M, Xu L, Ma, H. Electrochemical non-enzymatic glucose sensor using ionic liquid incorporated cobalt-based metal-organic framework. Microchem J. 2020;159:105343.
71. Sun S, Tang Y, Wu C, Wan C. Phytic acid functionalized ZIF-67 decorated graphene nanosheets with remarkably boosted electrochemical sensing performance. Anal Chim. Acta 2020; 1107: 55-62.
72. Chiu WT, Chang TFM, Sone M, Tixier-Mita A, Toshiyoshi H. Roles of TiO2 in the highly robust Au nanoparticles-TiO2 modified polyaniline electrode towards non-enzymatic sensing of glucose. Talanta 2020; 212:120780.
73. Geng D, Bo X, Guo L. Ni-doped molybdenum disulfide nanoparticles anchored on reduced graphene oxide as novel electroactive material for a non-enzymatic glucose sensor. Sens. Actuators B Chem. 2017; 244:131-141.
74. Hussein BA, Tsegaye AA, Shifera G, Taddesse AM. A sensitive non-enzymatic electrochemical glucose sensor based on a ZnO/Co_3O_4/reduced graphene oxide nanocomposite. Sens Diagn. 2023; 2(2): 347-360.